

# Long-term evolution of isolated $N$ -body systems

Holger Baumgardt,<sup>1</sup> Piet Hut,<sup>2</sup> Douglas C. Heggie,<sup>3</sup>

<sup>1</sup>*Department of Astronomy, School of Science, The University of Tokyo, 7-3-1 Hongo, Bunkyo-ku, Tokyo 113-0033, Japan*

<sup>2</sup>*Institute for Advanced Study, Princeton, NJ 08540, USA*

<sup>3</sup>*Department of Mathematics and Statistics, University of Edinburgh, King's Buildings, Edinburgh EH9 3JZ, UK*

Accepted . Received ; in original form

## ABSTRACT

We report results of  $N$ -body simulations of isolated star clusters, performed up to the point where the clusters are nearly completely dissolved. Our main focus is on the post-collapse evolution of these clusters. We find that after core collapse, isolated clusters evolve along nearly a single sequence of models whose properties are independent of the initial density profile and particle number. Due to the slower expansion of high- $N$  clusters, relaxation times become almost independent of the particle number after several core collapse times, at least for the particle range of our study. As a result, the dissolution times of isolated clusters exhibit a surprisingly weak dependence on  $N$ .

We find that most stars escape due to encounters between single stars inside the half-mass radius of the cluster. Encounters with binaries take place mostly in the cluster core and account for roughly 15% of all escapers. Encounters between single stars at intermediate radii are also responsible for the build up of a radial anisotropic velocity distribution in the halo. For clusters undergoing core oscillations, escape due to binary stars is efficient only when the cluster center is in a contracted phase. Our simulations show that it takes about  $10^5$   $N$ -body time units until the global anisotropy reaches its maximum value. The anisotropy increases with particle number and it seems conceivable that isolated star clusters become vulnerable to radial orbit instabilities for large enough  $N$ . However, no indication for the onset of such instabilities was seen in our runs.

**Key words:** methods: numerical - celestial mechanics, stellar dynamics - globular clusters: general.

## 1 INTRODUCTION

It is one of the great challenges of numerical astrophysics to understand the dynamical evolution of globular clusters and other collisional systems (as e.g. galactic nuclei; galaxy clusters). So far however, it is not possible to perform simulations of such rich systems by direct summation techniques and one has to rely on a statistical modeling. This is still the case, despite recent progress in the development of faster computers, like e.g. the GRAPE computer series (Makino 2001, 2002).

Statistical modeling of globular clusters includes different techniques like Fokker-Planck, Monte Carlo and Gaseous model simulations. There has been substantial progress in recent years in improving the reality of such models and comparing them with  $N$ -body models or comparisons between different statistical methods show good agreement in many cases (Takahashi & Portegies-Zwart 2000, Giersz & Spurzem 2000). Nevertheless the validity of such codes for real globular clusters should be checked further, due to the complexity of the physical processes involved and the fact

that the gap between the largest published  $N$ -body models (which are of order  $3 \cdot 10^4$ ), and the number of stars in real globular clusters (roughly  $N = 10^6$ ) is still large.

Isolated star clusters are an ideal environment to test star cluster evolution. These systems are sufficiently simple, but nevertheless show many phenomena that are also seen in real globular clusters. Although simulations of isolated clusters are not directly applicable to real stellar systems, they are nevertheless highly relevant. Borrowing an example from stellar evolution, such calculations play the role that polytropic models have played there historically. While rather unrealistic physically, they did shed considerable light on the basic aspect of stellar structure, and in addition they served as useful comparison material when trying to interpret the results of the far more detailed numerical evolution models. Models for isolated clusters have the same dual role in stellar dynamics, they show some of the major physical effects occurring in long-term dynamical evolution, and provide templates against which more detailed models can be interpreted. A large amount of research has therefore been devoted to the study of isolated clusters.

It has been known for a long time that star clusters undergo a contraction of their center as a result of heat transfer from the cluster core to the halo (Antonov 1962, Lynden-Bell & Wood 1967). For isolated, single-mass clusters, this core collapse takes roughly 17 initial relaxation times until completion (Takahashi 1995), and the core collapse evolution is thought not to change very much in the presence of an external tidal field (Giersz & Heggie 1997). Lynden-Bell & Eggleton (1980) found that the core collapse proceeds from the outer to the inner parts and leaves behind a power-law debris of material with density exponent in the range  $\alpha = -2$  to  $-2.5$ . Although core collapse strongly influences the structure of the inner parts, one usually assumes that the overall properties of the system are determined more by the half-mass radius, and the core adjusts itself in post-collapse so as to balance the tendency of the halo to recollapse.

Core collapse will be reversed if a central energy source is present (Hénon 1975), and it is normally assumed that binary stars, which are either primordial or form during core collapse and harden as a result of encounters with field stars, provide this heat source (Aarseth 1971, Heggie 1975) in real star clusters. The number of binaries necessary to drive the cluster evolution is found to be quite small. Goodman (1984) estimated from his gaseous model calculations that their number drops with the number of cluster stars as  $N_b \propto N^{-0.3}$  and that in the mean only  $N_b = 0.5$  binaries are necessary to drive the evolution of a cluster with  $N = 10^6$  stars. This has been partly confirmed by Giersz & Heggie (1994b) in their  $N$ -body simulations of small- $N$  clusters. They found that only few binaries are present in the core, but their number seemed to increase with the particle number. They noted however that some of their binaries might be temporary ones which contribute nothing to the energy generation of the core.

Stars scattered out of the cluster center create an radially anisotropic velocity profile in the cluster halo (Larson 1970). Cohn (1984) found that a cluster starts to become anisotropic in its outer parts already early on in the pre-collapse phase, while Spitzer & Shapiro (1972) have argued that the anisotropy extends down into the core as a consequence of its collapse. This was later confirmed by Takahashi (1995) and Drukier et al. (1999) for the late stages of core collapse. For post-collapse clusters, Takahashi (1996) found that they are isotropic in their center and the anisotropy increases monotonically towards the halo.

Encounters of stars in the cluster center also lead to the escape of stars. Hénon (1960) has shown that stars in isolated systems do not escape by distant encounters, but only due to close encounters with other stars. Despite their small numbers, it is generally believed that binaries play an important role in the production of escapers and contribute to the development of an anisotropic velocity profile in the cluster halo.

So far, most simulations of isolated star clusters were concerned only with the early stages up to core collapse or the immediate re-expansion phase. Nearly nothing is known about how clusters evolve when substantial mass-loss sets in. One reason for this neglect is that the escape of stars from isolated clusters happens very slowly and on a timescale which increases rapidly as the clusters expand. In addition, large-angle scatterings are neglected in Fokker-Planck meth-

ods and can only be studied by  $N$ -body or Monte Carlo simulations.

Hence, although highly desirable, it is difficult to verify the predictions of Fokker-Planck or Gaseous models by direct  $N$ -body simulations. We therefore present in this paper the first  $N$ -body simulations of medium sized isolated star clusters which follow the evolution until near complete disintegration.

## 2 DESCRIPTION OF THE RUNS

We simulated the evolution of clusters containing between  $N = 128$  and 8192 equal-mass stars, increasing the particle numbers by successive factors of 2. Our clusters followed Plummer profiles initially and we did not impose a cut-off radius when the Plummer models were created. Small- $N$  runs were made with the collisional Aarseth  $N$ -body code NBODY6 (Makino & Aarseth 1992, Aarseth 1999) on a Pentium PC workstation. The 8K run was made with the NBODY6++ code (Spurzem 1999, Spurzem & Baumgardt 2002), which is a parallelized version of NBODY6. It was made on a Cray T3E parallel computer using 8 processors. Though these  $N$  are not large by the standards of current more realistic simulations, the computations are at least as time-consuming.

During the runs, we recorded the positions and velocities of all stars at regular intervals. In the first 100  $N$ -body time units, the output time  $\delta T$  was equal to one initial crossing time. Later, time-intervals were equally spaced in  $\log T$ . At each data output, we determined the number of bound stars, the lagrangian radii of the members (measured relative to the density center) and the velocity structure of the bound stars. We also calculated a scaled time according to

$$T_{Scale} = \int_0^{T_{NBODY}} \left( \frac{r_h(0)}{r_h(t)} \right)^{3/2} dt, \quad (1)$$

where  $r_h$  is the half-mass radius of the bound cluster. This time takes the expansion of the cluster into account (but not the mass-loss), and measures how much time has passed in comoving coordinates. Data was also stored every 2.828 timeunits in scaled time.

The runs were performed for a maximum time of  $T_{Max} = 10^{16}$   $N$ -body units. In order to follow the evolution up to the point where nearly all stars are unbound, we had to rescale the whole system when its size became too large. Otherwise the simulations would have come to a halt due to numerical difficulties in NBODY6. Rescaling was done by calculating the sum of the potential energies of all stars, excluding the internal energy of regularised binaries. The positions and velocities of all stars were then rescaled such that the total potential energy after rescaling was equal to  $E_{Pot} = -1/2$ . The cluster centers were also moved back to the origin and the mean cluster velocity was subtracted from all stars. This recentering did not influence the cluster membership. In general, the whole integration could be covered by two rescalings.

Bound stars were determined in the following way: We first calculated the potential energy of each star with respect to all other stars. Kinetic energies were then calculated relative to the motion of the cluster center, which was taken from a previous iteration, or, at the start of the run, assumed

**Table 1.** Details of the performed  $N$ -body runs.

$N$	$N_{Sim}$	$T_{Finh}$	$\langle N_{Tmax} \rangle$	$T_{CC}$	$T_{Half}$
128	64	$2.8 \cdot 10^{12}$	–	70.7	$6.75 \cdot 10^4$
256	64	$1.3 \cdot 10^{14}$	–	104.7	$6.70 \cdot 10^4$
512	40	$1.2 \cdot 10^{15}$	12.7	169.7	$7.56 \cdot 10^4$
1024	20	$1.0 \cdot 10^{16}$	28.5	360.3	$9.05 \cdot 10^4$
2048	10	$1.0 \cdot 10^{16}$	49.4	587.5	$1.39 \cdot 10^5$
4096	5	$1.0 \cdot 10^{16}$	100.5	1031.2	$2.29 \cdot 10^5$
8192	1	$1.0 \cdot 10^{16}$	182.0	1839.2	$3.79 \cdot 10^5$

to be zero. The mean cluster motion was then determined from the bound stars (i.e. those with total energies  $E < 0$ ) and in the following iteration potential energies were calculated with respect to the bound stars only. This method was repeated until a stable solution for the cluster motion and the number of bound stars was found. From the cluster members, we determined the position of the density center and the lagrangian radii, using the method of Casertano & Hut (1985). Unbound stars were not removed from the simulations, although for the analysis in this paper we will restrict ourselves to the bound stars. We note that throughout the paper, the term cluster will be used for the system of bound stars only. We also note that using unbound stars for the calculation of the potential energy or the position of the density center would make little difference to our results, since they contribute little to the potential energy and also have only a small weight in the calculation of the density center.

Table 1 gives an overview of the simulations. It shows the number of cluster stars  $N$ , the number  $N_{Sim}$  of simulations performed, the time  $T_{Finh}$  when half the simulations had stopped (explained below), the number of stars still bound at  $10^{16}$   $N$ -body time units and the core collapse and half-mass times of the models.

Runs were terminating before  $T_{Max}$  due to either difficulties in the numerical integration or because our routine for the membership determination couldn't find bound stars. This happened for example when a cluster consisted of only two or three stars and these were merged by NBODY6 to form an hierarchical system. Runs which finish before  $T_{Max}$  might bias our results, so results obtained for  $T \geq T_{Finh}$  should be treated with caution. However, Table 1 shows that only results for small- $N$  clusters might be biased and these also only for the very late stages of the evolution.

Throughout the paper we will use  $N$ -body units, so the constant of gravitation, initial cluster mass and energy are given by  $G = 1$ ,  $M = 1$  and  $E_C = -0.25$  respectively.

### 3 RESULTS

#### 3.1 Pre-collapse evolution

We will start our analysis by discussing the pre-collapse evolution of the clusters. Fig. 1 compares the evolution of different models after the  $N$ -body time units were divided by the half-mass relaxation time (Spitzer 1987)

$$T_{RH} = 0.138 \frac{\sqrt{N} r_h^{3/2}}{\sqrt{m} \sqrt{G} \ln \gamma N}, \quad (2)$$

where  $N$  is the initial number of cluster stars,  $m$  their mean mass,  $r_h$  the initial half-mass radius of the cluster,  $\gamma$  a

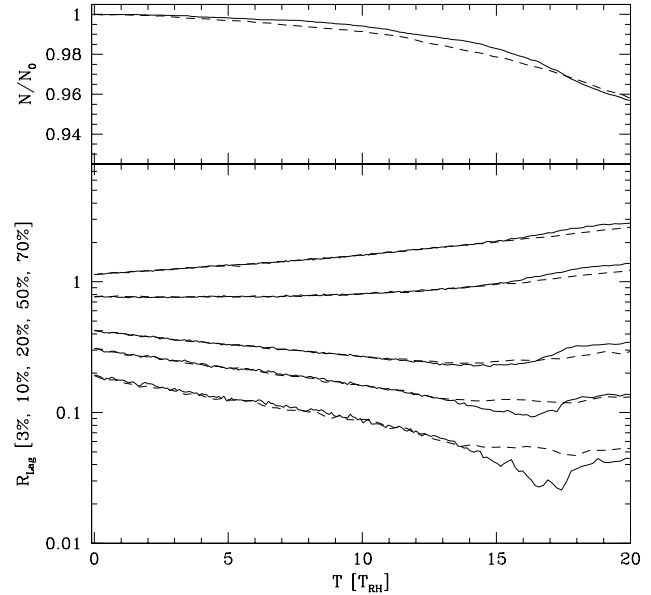


**Figure 1.** Pre-collapse evolution of clusters containing  $N = 1024$  (dashed) and  $N = 4096$  (solid line) stars. The bottom panel shows the evolution of the lagrangian radii, the top panel shows the evolution of the bound mass. Time is scaled by the initial relaxation time. The lagrangian radii evolve in the same way in both models until shortly before core collapse.

constant in the Coulomb logarithm (discussed below), and  $G$  the constant of gravitation.

The bottom panel shows lagrangian radii containing between 3% to 70% of the bound stars, calculated by averaging the radii from individual runs. The collapse of the clusters and the following re-expansion can be clearly seen. Core collapse is achieved in approximately 17 initial relaxation times, which agrees well with published results from anisotropic Fokker-Planck runs (Takahashi 1995, Drukier et al. 1999). For most of the pre-collapse phase good agreement in the evolution of the lagrangian radii for different  $N$  can be seen. Significant deviations occur only shortly before core collapse, when heat input by binaries starts to influence the core evolution. Giersz & Spurzem (1994) found that high- $N$  clusters undergo a core collapse which is deeper and happens at later times since binaries in low- $N$  clusters have to create less energy to stabilise the cluster core from further contraction. Goodman (1987) found in his gaseous model calculations that high- $N$  clusters have a smaller core radius also in the post-collapse phase. As can be seen, these results agree very well with the results of our  $N$ -body calculations. Fig. 1 shows that the core radii of high- $N$  models remain smaller during the post-collapse phase, while their intermediate radii, probably as a result of the stronger energy generation in the core, are larger.

The outer radii are expanding right from the start of the simulations. In agreement with Cohn (1984), we find that the halos become anisotropic already during the pre-collapse phase (Fig. 17), so the pre-collapse expansion is at least partially driven by stars ejected from the cluster cores. These stars must be ejected by two-body encounters between

single stars, as no binaries are present in the clusters before core collapse.

Comparing the evolution of models with different  $N$  allows us to determine the value of the Coulomb logarithm used in eq. 2. From a fit of the Lagrangian radii, we typically obtained values between  $\gamma = 0.05$  and  $0.2$ , depending on which radii and particle numbers are compared. These values are similar to the value of  $\gamma = 0.11$  obtained by Giersz & Heggie (1994a) from a comparison of  $N = 500$  and  $N = 2000$  models. Since the number of our simulations is relatively small, these differences are probably within the statistical error.

The upper panel of Fig. 1 depicts the mass-loss. The mass-loss rate increases monotonically towards core collapse and about 3% of the mass is lost in pre-collapse. There is a trend that the 4K-model loses mass at a slightly smaller rate in the beginning, and this effect can also be seen if we compare other models. The reason could be that stars in isolated models escape only by very close encounters, for which Hénon (1960) found that they lead to a scaling of the lifetime proportional to  $N$  rather than  $N/\log(N)$ .

### 3.2 Post collapse expansion

The post-collapse expansion of an isolated cluster is usually assumed to be self-similar. In this case, its evolution is characterized by the following two equations:

$$\begin{aligned} \frac{dM(t)}{dt} &= -k_1 \frac{M(t)}{t_{rh}} \\ \frac{dr_h(t)}{dt} &= k_2 \frac{r_h(t)}{t_{rh}} \end{aligned} \quad (3)$$

If the variation in the Coulomb logarithm of the relaxation time can be neglected, the solution for the mass-loss and the half-mass radius is given by:

$$\begin{aligned} M(t) &= M_0 (t/t_0)^{-\nu} \\ r_h(t) &= r_{h0} (t/t_0)^{(2+\nu)/3} ; \end{aligned} \quad (4)$$

where  $t_0$  is the time of core collapse and  $\nu$  a constant. Goodman (1984) obtained values of  $\nu$  ranging from 0.0258 to 0.100 for the evolution of his homologous sphere. Similar values were also found by Giersz & Heggie (1994b) in their  $N$ -body simulations of small- $N$  clusters. On the other hand, Drukier et al. (1999) found strong deviations from a  $r \propto t^{2/3}$  scaling for clusters with  $N \geq 8000$  stars in their anisotropic Fokker-Planck simulations, especially for the outer radii. They attributed these changes to the buildup of a radially anisotropic velocity distribution in the cluster halos.

Fig. 3 shows the evolution of the Lagrangian radii as a function of  $N$ -body time in our simulations. We have shifted the  $N$ -body time units such that all clusters go into core collapse at the same time as the 4K model. Due to their smaller relaxation times, low- $N$  clusters need less time to reach core collapse and also expand quicker after core collapse, which can be seen most clearly in the evolution of the outer Lagrangian radii.

A strong increase of the outer radii might be expected since the halo density in a Plummer model drops off like  $\rho \propto r^{-5}$ , while for an isolated cluster with mass-loss one expects to find an equilibrium relation  $\rho \propto r^{-3.5}$  (Spitzer & Shapiro 1972). The build up of this halo will cause the outer

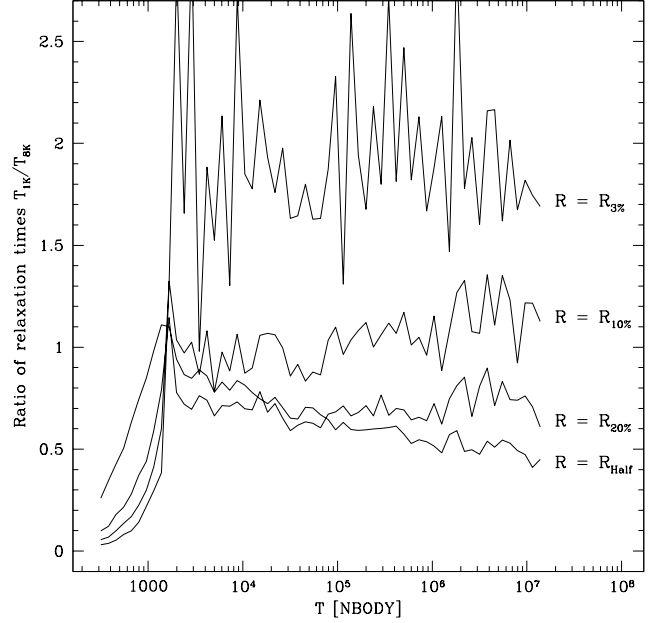


**Figure 2.** Ratio of the relaxation times of the 1K and 8K models at different radii. The 8K model has a smaller relaxation time in the core but a larger relaxation time in the halo. Relaxation times are approximately the same at the 10% radius, showing that the cluster expansion is driven from around this radius.

radii to expand and might also explain the increase seen by Drukier et al. (1999, their Fig. 6).

The quick expansion of low- $N$  clusters cannot be sustained indefinitely however, since, as a cluster expands, its relaxation time increases with it. Hence, the expansion of a low- $N$  cluster cannot go beyond a point where its relaxation time reaches the relaxation time of an high- $N$  cluster. After some time has passed in post-collapse expansion, one would therefore expect that high- $N$  clusters have smaller radii which compensate their large particle numbers, and that all clusters expand with the same rate. It can be seen in Fig. 3 that this is nearly the case.

Interestingly, from a comparison of different models, one can find a Lagrangian radius at which the relaxation time (estimated in a manner to be described) is the same for all models at the same time. In a sense this can be interpreted as the radius which drives the expansion. In order to estimate the relaxation time at a given Lagrangian radius  $r$  we use eq.(2) with  $r_h$  replaced by  $r$ . This does not take into account the fact that the mass within radius  $r$  varies with  $r$ , but since our purpose is to compare different models at the Lagrangian radius corresponding to the same fractional mass, this is not important. Fig. 2 shows the ratio of the relaxation times of the 1K and 8K clusters at 4 different radii as a function of time. Throughout the post-collapse evolution, both clusters have similar relaxation times at the 10% radius, although there is some tendency towards larger radii towards the end. Similar results are obtained from a comparison of other  $N$ . The expansion of isolated clusters may therefore be thought of as being driven from around the 10% radius. The cluster cores will adjust themselves and their energy generation to deliver the necessary energy, while relaxation times at radii

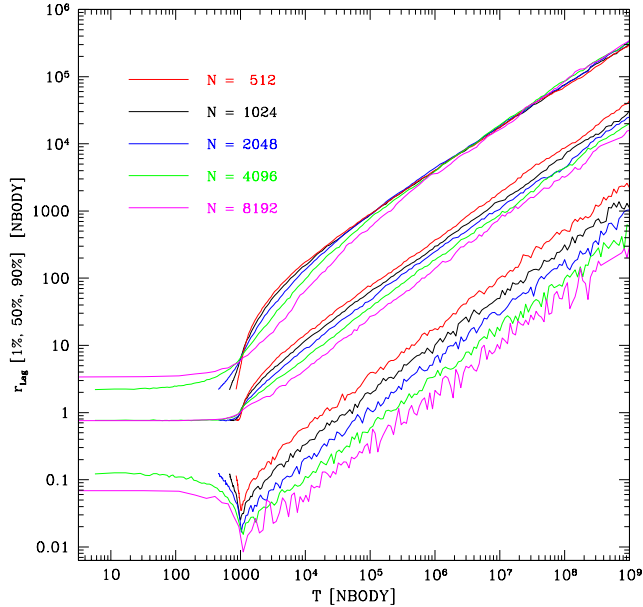


**Figure 3.** Evolution of the lagrangian radii for clusters with different initial particle numbers. Times are shifted such that all clusters go into core collapse at the same time. Low- $N$  clusters expand quicker after core collapse, and due to this faster expansion their relaxation times reach those of high- $N$  clusters. After  $10^5$   $N$ -body time units, all clusters do therefore expand with the same rate.

outward from the 10% radius are too large to influence the expansion much.

Although it is clear from Fig. 3 that the post-collapse expansion cannot be strictly self-similar, the inner lagrangian radii up to the half-mass radius expand regular enough to be fitted by a relation like eq. 3. Fitting the evolution of different lagrangian radii and the mass-loss curve between  $10^3$   $N$ -body time units and  $10^8$   $N$ -body time units ( $10^4$  to  $10^8$  for  $N \geq 4096$ ) gives the  $\nu$ -values shown in Table 2. For all  $N$ ,  $\nu$  drops with increasing distance from the cluster center, so that the core radii show the fastest expansion. The reason for this will be discussed in the next section.

Our values for the expansion of the half-mass radius agree fairly well with the values found by Goodman (1984) and Giersz & Heggie (1994b), despite the fact that different times were used by Giersz & Heggie (1994b) to obtain them and the scatter in  $\nu$  is fairly large for our high- $N$  runs. Unfortunately no comparison values are available for the inner lagrangian radii. The best agreement with the  $\nu$ -values derived from the mass-loss curve is achieved for the 10% and 20% lagrangian radii. Since escapers are created mainly between these radii (see section 3.4), a close correspondence in the behavior with time might be expected.

Another interesting result of Table 2 is that the  $\nu$  values derived from the mass-loss curve increase with  $N$ , which means that high- $N$  clusters lose mass faster than clusters with smaller particle numbers. This is in contrast to a naive application of standard relaxation theory, in which it is assumed that  $\nu$  is independent of  $N$  (eqs. 4). A large part

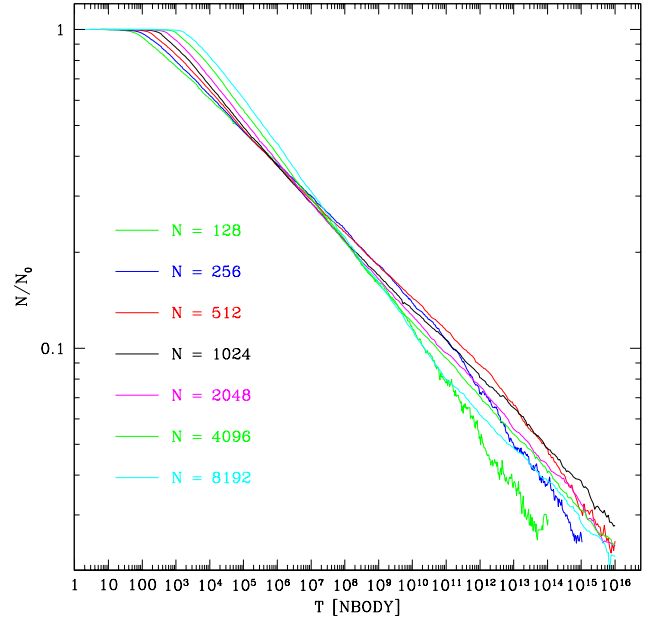


**Figure 4.** Fraction of bound mass as a function of  $N$ -body time. Shown are clusters containing between  $N = 128$  to  $N = 8192$  stars. Although low- $N$  clusters have initially smaller relaxation times and start losing mass earlier, curves for different  $N$  meet each other at about  $10^7$   $N$ -body time units. Afterwards, high- $N$  models contain a smaller amount of mass at any given time, except for models with  $N < 512$ .

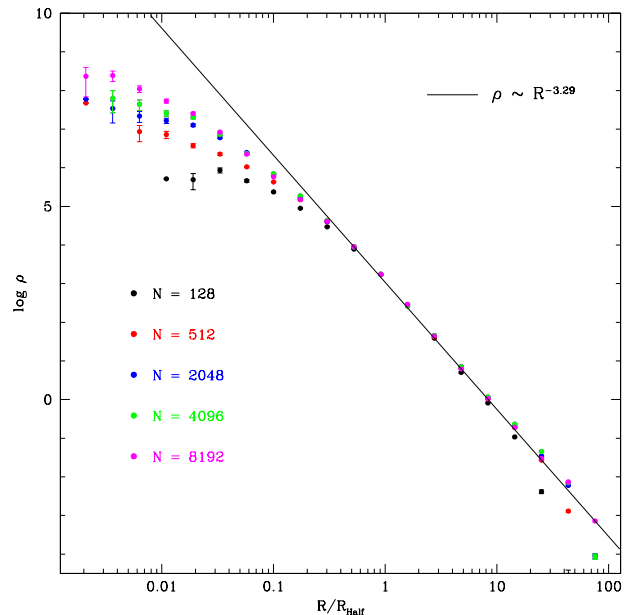


**Figure 5.** Density profiles for clusters starting with  $N = 128$  to  $N = 8192$  stars. Radii are given in units of the half-mass radius and densities are adjusted to be the same for all  $N$  at the half-mass radius. The solid line shows a density profile proportional to  $\rho \propto R^{-3.29}$ . It gives a good fit to the halo profiles, especially for large  $N$ .

**Table 2.** The parameter  $\nu$  determined from the mass-loss and the expansion rate of four different lagrangian radii as a function of the particle number  $N$ . Closest agreement with a self-similar expansion is achieved if the expansion of the 10% radius is compared with the mass-loss rate.

$N$	128	256	512	1024	2048	4096	8192
$\nu_M$	0.10	0.11	0.11	0.13	0.13	0.14	0.14
$\nu_{r3}$	0.16	0.16	0.17	0.16	0.15	0.17	0.22
$\nu_{r10}$	0.13	0.11	0.14	0.14	0.13	0.11	0.13
$\nu_{r20}$	0.08	0.12	0.13	0.11	0.08	0.05	0.09
$\nu_{r50}$	0.08	0.09	0.07	0.02	0.01	0.06	0.09

of this discrepancy can be explained by the higher concentration of high- $N$  clusters, which breaks the homology and makes  $k_1$  (eq. 3), and therefore  $\nu$ , increase with  $N$ .

Plotting the bound mass as a function of time (Fig. 4) shows that low- $N$  clusters start losing mass quicker due to their earlier core collapse, but that the increase in  $\nu$  is sufficient to reverse this after about  $10^7$   $N$ -body time units. Afterwards, high- $N$  runs contain a smaller fraction of their initial mass at a given  $N$ -body time, except for runs with  $N < 512$  which are affected by the increasing incompleteness towards the end.

Finally, Fig. 3 (and also Fig. 14) shows that our 8k-model undergoes core oscillations up to about  $10^4$   $N$ -body time units, when the number of cluster stars drops below 6700. The minimum required mass for core oscillations seems therefore to be of order 7.000, which agrees very well with results obtained by Goodman (1987) from his conducting gas sphere calculations. Only slightly larger values were obtained by Drukier et al. (1999) and Breeden et al. (1994), who found a lower limit of  $N \geq 8000$ .

### 3.3 Density profile in post-collapse

Fig. 6 depicts the relative sizes of the different radii for the 2K and 8K models in greater detail. The time of the 8K model is rescaled by the initial relaxation time to match the relaxation time of a 2K model, and radii are scaled by the actual 20% radius. The build up of the halo is happening very slowly for both  $N$  and is complete only after about  $10^5$   $N$ -body time units, corresponding to  $10^3$  initial relaxation times. By this time, the structure of the clusters outside the 20% radius is very similar for both  $N$ . Afterwards, the outermost radii in the 2K model start to decrease. This decrease is caused by the recoil motion of the clusters due to escaping stars. Due to this recoil, weakly bound stars in the cluster halos gain positive energies relative to the cluster centers and escape. The recoil motion is larger and more erratic for low- $N$  clusters since a single star carries a larger fraction of the total cluster mass. Their halos will therefore be truncated at smaller radii.

In contrast to the halo, the post-collapse profile inside the half-mass radius is established already during core collapse and changes only little afterwards. The core radii of high- $N$  clusters are more concentrated relative to the 20% radius than those of low- $N$  clusters. Giersz & Spurzem (1994) found that in low- $N$  models binaries have a higher chance to form and have to release less energy to prevent the core from contracting. They studied mainly the pre-collapse phase, however, given the similar density profile, the same

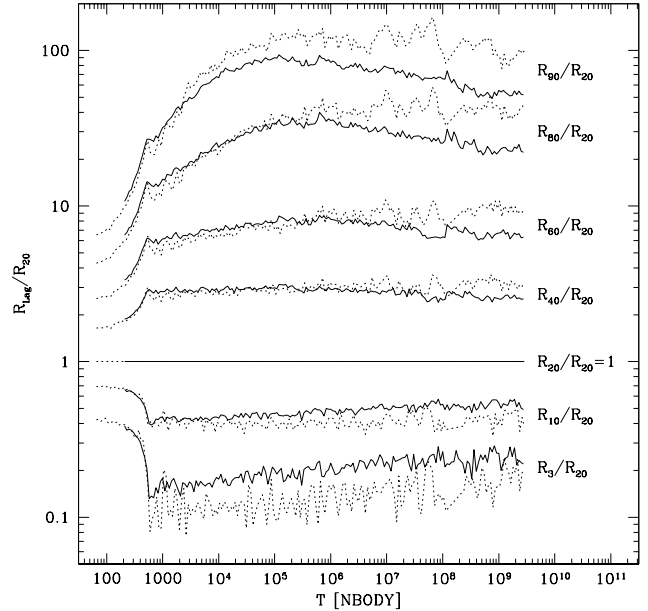


**Figure 6.** Ratio of the lagrangian radii relative to the 20% radius for clusters with  $N = 8192$  (dashed line) and  $N = 2048$  (solid line) stars. The time in the 8K model is rescaled by the relaxation time to that of the 2K model. Halos expand after core collapse until their build-up is reversed by the removal of weakly bound stars from the recoil motion of the center due to escaping stars. The cores are expanding slowly throughout the simulation because of increased binary activity in the center.

conditions should prevail in the post-collapse phase. The larger core size of low- $N$  clusters is therefore due to the stronger binary activity in their centers. Consequently, as the clusters evolve and lose mass, their core radii increase with time.

Fig. 5 shows the density profiles at the time the cluster halos reach their maximum expansion relative to the 20% radius. Radii are given in units of the half-mass radius and densities are adjusted such that they are the same at the half-mass radius. In the halo, the density profiles of all clusters follow power-law distributions  $\rho \propto R^{-\alpha}$  with slope  $\alpha = 3.29$ . Deviations from this occur only in the outermost bins, where small- $N$  clusters have steeper profiles because of the recoil motion from escaping stars, which effectively truncate the clusters at a certain radius.

Our value for  $\alpha$  is not far from the theoretical prediction by Spitzer & Shapiro (1972), who found  $\alpha = 3.5$  for the halo density of an isolated star cluster. Similar slopes were also found by Lightman & Shapiro (1978) and by Takahashi (1996) in his Fokker-Planck simulations of anisotropic post-collapse clusters.

The transition between the halo and the inner parts happens at around  $R = 0.4$  half-mass radii. Inward from there, clusters have shallow density profiles which become steeper for increasing  $N$ . Inagaki & Lynden-Bell (1983) and Takahashi (1995) found that the inner profiles can be fitted by power-law distributions with slopes of  $\alpha = 2.0$  and  $\alpha = 2.23$  respectively. Our profiles do not strictly follow power-laws, but can be fitted by them over a restricted range in  $R$ .

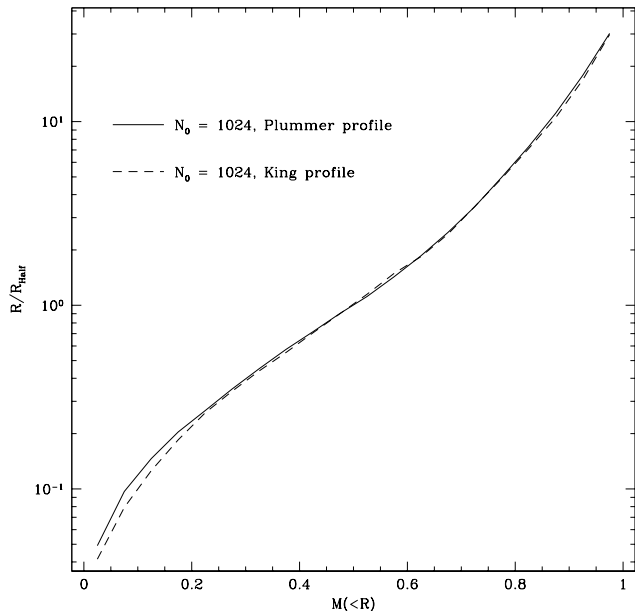


**Figure 7.** Cumulative mass distribution at half-mass time for clusters starting with different density profiles. Clusters starting with Plummer profiles are shown by a solid line, clusters starting with King  $W_0 = 3.0$  profiles by a dashed line. The distributions at half-mass time agree approximately with each other since the cluster expansion has erased the memory of the starting condition.

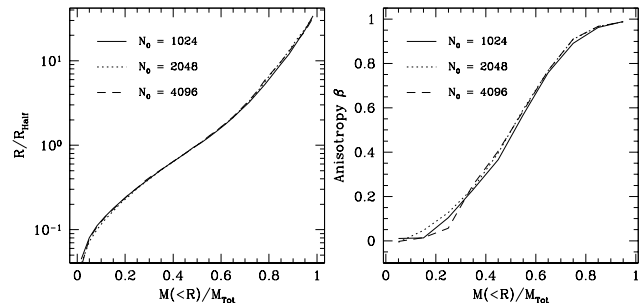
For the 4K and 8K models, an increase of  $\rho \sim R^{-2.33}$  gives a good fit between 0.02 and 0.3 half-mass radii, which is not too different from the result of Takahashi (1995). Given the relatively small number of stars in our simulations, and the fact that the profiles have not reached a limiting profile even for our largest  $N$ , it might be possible that a single power-law profile is reached in the centers of large- $N$  clusters.

### 3.4 Evolution along a single sequence of models ?

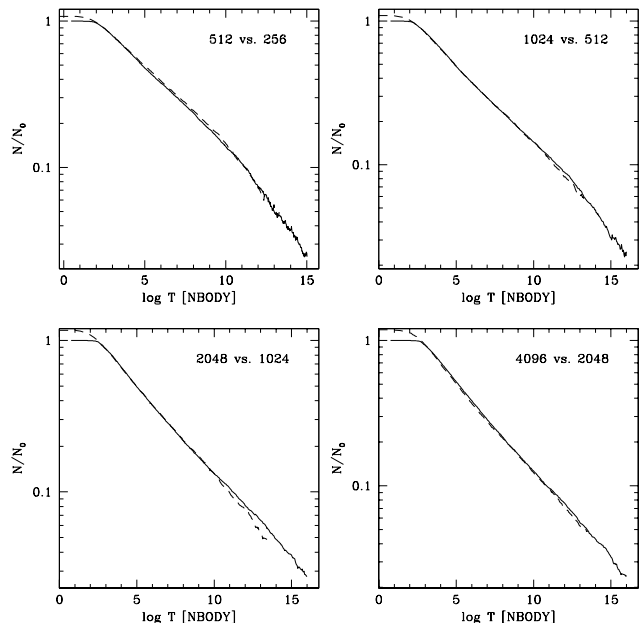
In the expansion phase after core collapse, the space that the clusters initially occupied becomes a vanishing fraction of their actual volume. One might therefore ask if the density profile after a large enough time has passed still depends on the initial profile. In order to test this assumption, we made a set of 8 comparison runs which started from King  $W_0 = 3.0$  profiles and had  $N = 1024$  stars initially.

Fig. 7 compares the cumulative mass distribution of the King-models with the  $N = 1024$  Plummer-model, after both have lost half their initial mass (note that the clusters have expanded by about a factor of 100 by this time). A cumulative distribution has the advantage that it better shows the behavior of the bulk of the stars. It can be seen that the mass profiles of both clusters agree very well with each other. Similar comparisons at other times give the same agreement, provided the time is much larger than the core collapse time. The density distribution of isolated clusters long after core collapse becomes therefore independent of their initial density profile.

Similarly one might ask whether the density profile or any other cluster parameter at a given particle number still



**Figure 8.** Distribution of density and anisotropy  $\beta$  of clusters starting with different initial particle numbers by the time 512 stars are bound. Radii are scaled by the half-mass radius.  $\beta$  is calculated as explained in section 3.7. Both the mass and anisotropy profiles are independent of the initial particle number  $N_0$ .



**Figure 9.** Evolution of the number of bound stars for different clusters. Radii are rescaled such that the size of high- $N$  clusters when they have 45% bound stars is equal to the size of low- $N$  clusters with 90% bound stars.  $N$ -body time units are scaled by  $r_h^{3/2}$ . After this rescaling, the bound mass evolves similar in both cases, showing that the evolution is independent of the initial particle number.

depends on the initial number of cluster stars. Fig. 8 depicts the density and anisotropy profile as a function of enclosed mass by the time 512 stars remain bound, for clusters starting between  $N_0 = 1024$  to  $N_0 = 4096$  stars. The density and anisotropy profiles agree well with each other for any radius, and similar plots at other times also give excellent agreement between the runs.

We conclude that the cluster structure becomes independent of the initial particle number and density distribution after enough time has passed and is solely a function of the actual particle number. Clusters in late post-collapse

can therefore be characterised by only two parameters, as e.g. the current particle number and the half-mass radius. This would imply that isolated clusters evolve along a single sequence of profiles and that the evolution of clusters which started from different initial configurations is similar.

To check this assumption, we have a look at the evolution of bound mass with time. If clusters evolve along a single sequence, the evolution of low- $N$  clusters should be similar to that of high- $N$  clusters when they have reached the same number of stars. Fig. 9 compares the mass-loss rate of small- $N$  clusters with clusters that had initially twice as many stars. High- $N$  runs are rescaled such that the cluster sizes when 45% of the stars remain bound are equal to the sizes of the low- $N$  clusters when 90% of their stars are bound. The time is also shifted such that clusters reach 90% and 45% bound stars at the same time. It can be seen that we obtain a very good fit for the evolution of bound mass with time. The fit is best when many simulations were made as e.g. in cases with  $N = 512$  and  $N = 1024$ . Deviations occur, if at all, only at the end of the runs when the particle numbers are small. We conclude that isolated clusters evolve along a single sequence of models.

### 3.5 Escape of stars

It was shown by Hénon (1960) that stars can escape from isolated clusters only due to close encounters with other stars or binaries. If close encounters are the dominant escape mechanism, most stars should escape from the inner cluster regions, where the density of stars is highest and close encounters between stars should happen most often, though the potential well is deepest.

In our simulations, we checked the energy of each star when its regular force in NBODY6 was calculated. In order to do this, potential energies were calculated with respect to all stars and the kinetic energy was calculated relative to the cluster velocity from the time of the last data output. The time and radius where stars acquired positive energies were noted and we will refer to this radius as the ‘scattering distance’  $R_{Scatt}$ . If stars still had positive energies after their distance from the cluster center had increased by a factor of two compared to the scattering distance, we assumed that the star was successfully scattered out of the cluster and measured its excess energy above the  $E = 0$  energy threshold. Stars that fell below  $E = 0$  before they reached twice the scattering distance were not counted as escapers.

Fig. 10 shows, as an example for a low- $N$  cluster, the distribution of energies against scattering radius for the  $N = 512$  star models. The energies are expressed in terms of the one-dimensional velocity dispersion of all bound stars  $1kT = 2/3 \langle E_{Star} \rangle$  and the distances are measured in units of the 10% radius. One can notice three different concentrations in this diagram. Stars escaping due to single-star encounters have typical energies of a few tenths of  $1kT$  and acquire the escape energies at distances around the 10% lagrangian radius. Single-star escapers coming from distances closer to the cluster center have higher energies since stars at smaller radii move with larger velocities and can therefore also create higher energy escapers. The most distant single star escapers come from around  $R = 10 R_{10\%}$ , which correspond roughly to the half-mass radius. Stars escaping due to single-star encounters form the majority of escapers.

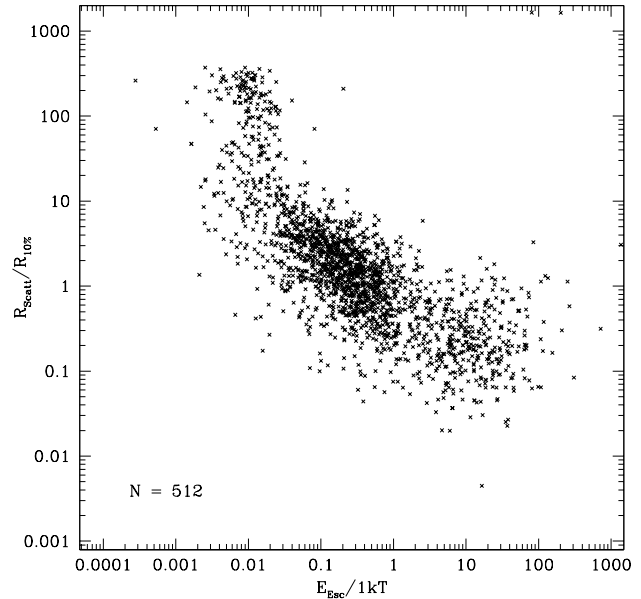


**Figure 10.** Distribution of escape energies against radius where stars become unbound for the  $N = 512$  star clusters. Plotted are all stars that escape before the half-mass time. The escape energies are measured after the stars have reached twice the scattering distance. Most stars escape due to encounters with single stars around the 10% lagrangian radius. Escapers with high energies come from encounters with binaries in the cluster cores.

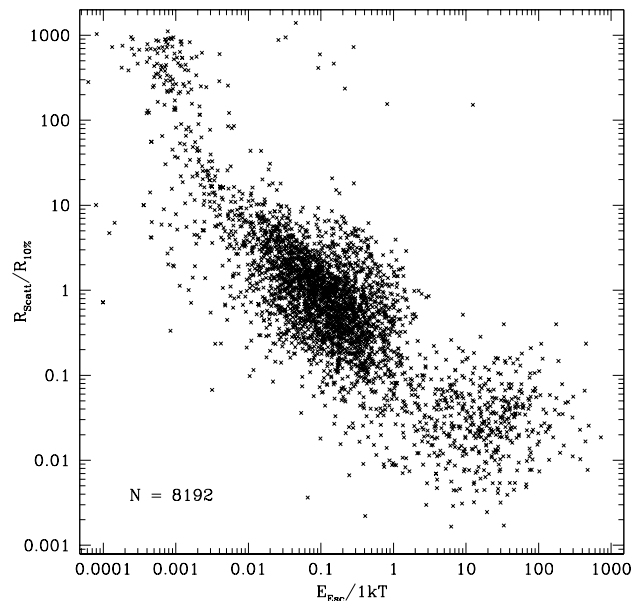


**Figure 11.** Same as Fig. 10 for the  $N = 8192$  cluster. The distribution is similar to the  $N = 512$  case, except that escapers from binary encounters are coming from much smaller distances.



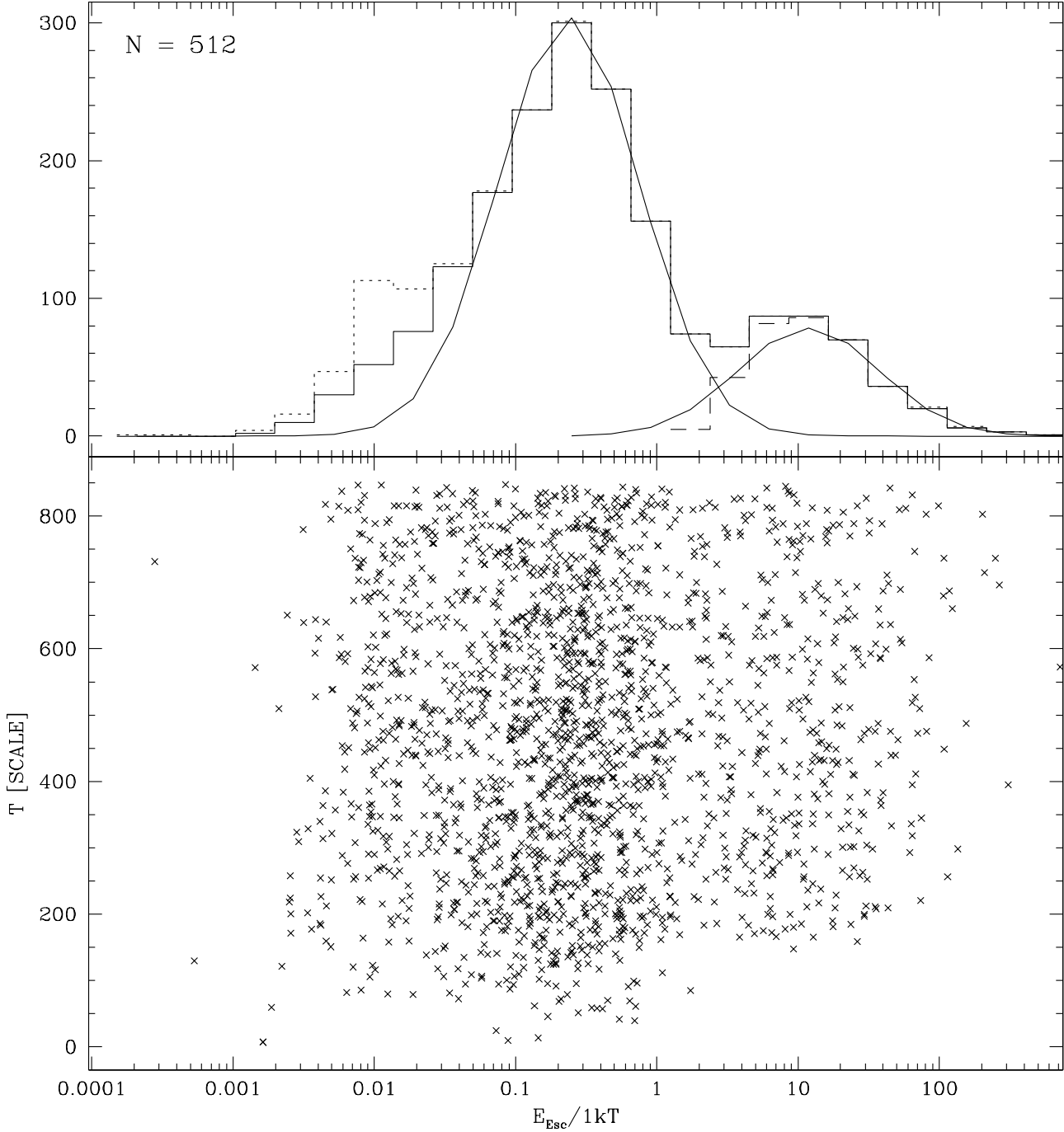


**Figure 12.** Distribution of escape energies as a function of scaled time for clusters with  $N = 512$  stars. Time is scaled according to eq. 1. The dotted line shows the distribution of all stars, the solid line shows the distribution after stars that escape due to the movement of the cluster have been subtracted. Escapers due to single star encounters follow roughly a gaussian distribution. The dashed line shows the remaining distribution after this gaussian has been subtracted from the high-energy escapers. Binary induced escape sets in only after core collapse and also follows roughly a gaussian distribution in energy.

Stars which escape because of binary-single star interactions are created only in the cluster cores and have typical energies between 2 and 100 kT. Since the energy of the escaper is coming from the internal energy of the binary, there is no dependence of the escape energy on the scattering radius. Although smaller in number, escapers due to binary

encounters carry away more than 95% of the total energy of escapers.

A third group of stars is created in the halos at distances larger than 10 half-mass radii. These stars escape since the cluster center moves erratically as a result of the recoil from

high energy encounters in the core, which will unbind loosely bound stars.

A similar plot for the 8K model (Fig. 11) shows that the energy of the single star escapers changes very little with particle number. In addition, the mean scattering distance remains the same. Escapers due to binaries are now well separated from the single star escapers. Their mean distance from the center has decreased by almost a factor of 10 due to the more concentrated core of the high- $N$  model.

Fig. 12 shows the distribution of escape energies as a function of scaled time (calculated according to eq. 1) for  $N = 512$ . Escape of high-energy stars sets in only after core collapse (happening at around  $T = 150$   $N$ -body time units). In agreement with Giersz & Heggie (1994a), we find that before core collapse, stars escape due to single star encounters only. The typical escape energies of single-star escapers show no variation with time and lie between 0.04 and 1kT. After stars escaping due to the movement of the cluster are taken out, the energy distribution can be fitted by a sum of two gaussians, which correspond to the two escape mechanisms. The majority of stars, typically about 80% to 85%, escape due to single-star encounters.

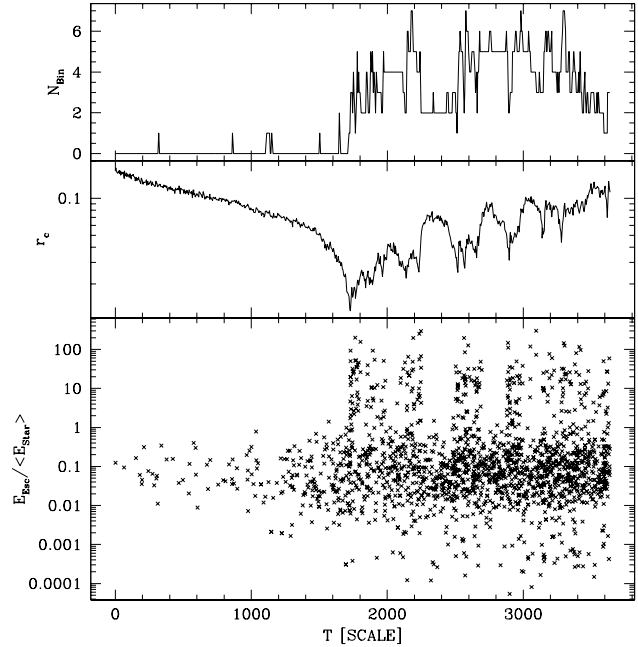
Fig. 13 shows the escape energies and escape times for stars in the 8K model. The energy distribution of stars escaping due to single-star and binary encounters is similar to the  $N = 512$  case. Escapers by binary encounters tend to have slightly higher energies than in the  $N = 512$  star case. The fraction of binary escapers is slightly smaller than in the  $N = 512$  case because the fraction of binaries compared to the number of cluster stars has decreased. The most striking difference is that in the 8K model, stars from binary encounters do not have a smooth distribution in time, but escape in several distinct phases.

Fig. 14 shows that these phases are linked to the core oscillations of the 8K model. Stars escape by binary encounters only when the cluster is in core collapse since the core density is much lower in an expansion phase where close encounters between binaries and single stars are unlikely. Stars escaping because of single-star encounters show much less variation with time as they are typically created at larger radii that change less due to the oscillations. Fig. 13 also shows that the rate at which single-star escapers are created is increasing during and after core collapse which could be the result of the increasing anisotropy. As a consequence, more loosely bound halo stars will travel through high-density regions where they have a high chance of being scattered to escape energies. In addition, the overall change in the density distribution can also increase the escape rate.

### 3.6 Binaries

Fig. 15 shows the number of bound binaries as a function of time. We assume that the number of binaries is equal to the number of regularised pairs in NBODY6, which should be the case except for transient encounters between cluster stars which are also regularised if they are close enough.

No binaries are present at the start of our simulations and they are created only during and after core collapse. The maximum number of bound binaries is reached after about 10 core collapse times. Throughout the post-collapse expansion, a few binaries are sufficient to drive the expansion of the clusters, even for clusters with several thousand stars.



**Figure 14.** Evolution of the escape energies (bottom panel), core radius (middle) and binary number (top) in the 8K model. Although binaries are present all the time, they are efficient in creating escapers only when the cluster is in core collapse.

The number of binaries increases with the number of cluster stars, while their fraction decreases. If the number of binaries is taken at the maximum value, the increase can be fitted approximately as  $N_{Bin} \propto N^{0.3}$ . This is comparable to the increase given by Giersz & Heggie (1994b), who found  $N_{Bin} \propto N^{0.2}$  after a few core collapse times had passed. Given the considerable scatter in our data and the fact that the binary number in our models is still rising after a few core collapse times, the agreement is satisfactory.

Comparison of the members of binary systems at successive times shows that the vast majority of them are not transient encounters but bound systems, especially for clusters with high particle numbers. In addition, the number of binaries in the core is increasing with the particle number in a similar way than the total binary number. Hence the number of active binaries needed to support the expansion of the clusters seems to rise with  $N$ , in contrast to Goodman's (1984) results from gaseous model calculations.

For later times, the binary fraction starts to drop again as the clusters contain fewer and fewer stars. This effect can best be seen for the high- $N$  runs. Runs with small particle numbers show almost no decrease, probably because at least one binary has to be present in the cluster core to drive the evolution. If this star is ejected, a new binary will be formed quickly, so a value of one forms a lower limit for the number of binaries (cf. Fig. 15).

The radial distribution of bound binaries is shown in Fig. 16. Although more concentrated than single-stars, a significant fraction of binaries can be found outside the core. Only one quarter of all binaries is located within the 3% lagrangian radius. Binaries outside the core are mostly ejected by three and four body interactions and move on very elongated orbits.

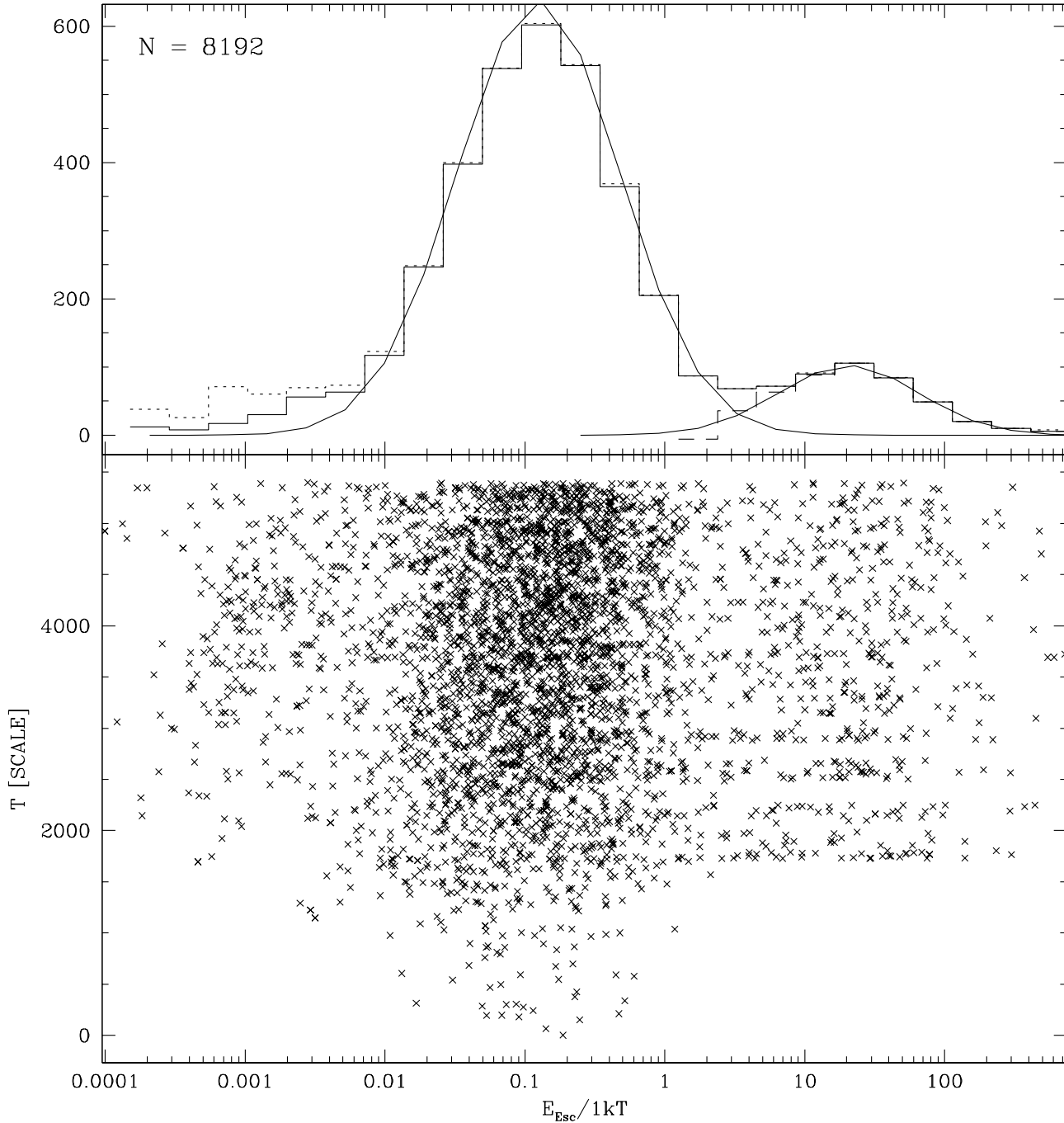


**Figure 13.** Same as Fig. 12 for  $N = 8192$  stars. The distribution of escapers is very similar to the  $N = 512$  case. However, stars that escape due to encounters with binaries do not escape continuously, but in several distinct phases which are related to the core oscillations of the cluster.

gated orbits. Subsequent passages through the cluster center will remove them from the cluster. Given the smaller density of stars and binaries in the halo, binary activity should be confined to the cluster centers.

### 3.7 Anisotropy

Fig. 17 shows the evolution of the mean anisotropy for clusters with  $N = 4096$  stars. To calculate the anisotropy, only bound stars are used. Following Binney & Tremaine (1987), we define the anisotropy parameter  $\beta$  as  $\beta = 1 - (\sigma_t^2 / 2\sigma_r^2)$ , which is half as large as the  $A$ -parameter used by Giersz & Spurzem (1994) and Takahashi (1996). The anisotropy

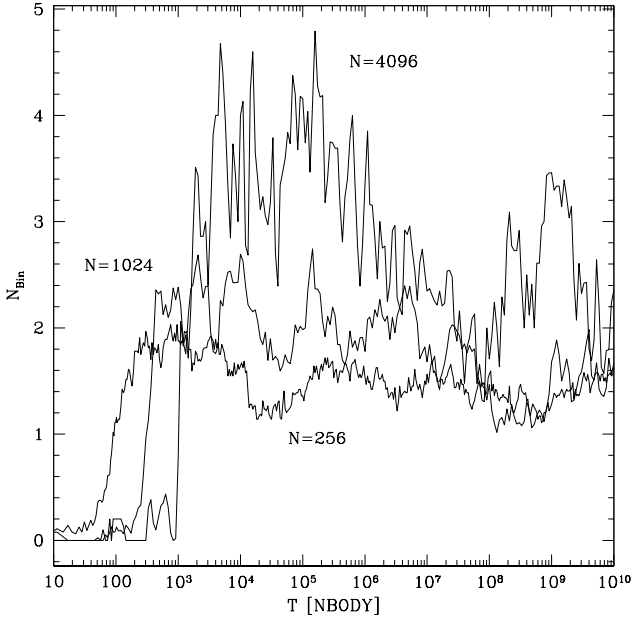


**Figure 15.** Number of bound, regularised binaries as a function of time. The binary number reaches a maximum after about  $10^4$  core collapse times. It is larger for high- $N$  clusters and decreases as the clusters lose stars.

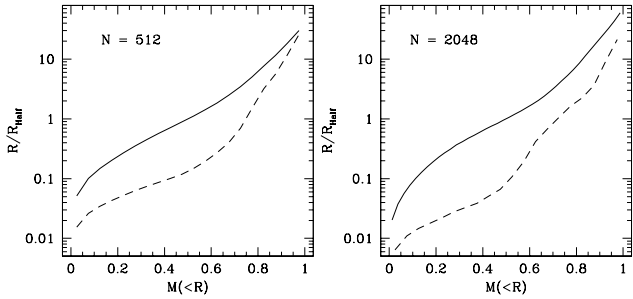


**Figure 16.** Radial distribution of binaries and single-stars for clusters containing  $N = 512$  and  $N = 2048$  stars respectively. Binaries (dashed) are more concentrated than single stars (solid line). In addition, binaries in high- $N$  clusters can be found at smaller radii.

rises from the start of the simulations and reaches a maximum after about  $10^6$   $N$ -body time units, corresponding to  $1.5 \cdot 10^4$  initial relaxation times. We find that the same number of initial relaxation times is required for other  $N$ . We also find a close agreement between the time when the clusters reach maximum anisotropy and the time when their halos reach maximum expansion relative to the inner radii. At this time, the outermost shells have become nearly 100% radially anisotropic. Clusters remain isotropic inside their 20% radius throughout the simulation, which agrees very well with results found by Takahashi (1996) from Fokker-Planck simulations.

One can see that the anisotropy is decreasing for very late times, which is the result of the increasing removal of

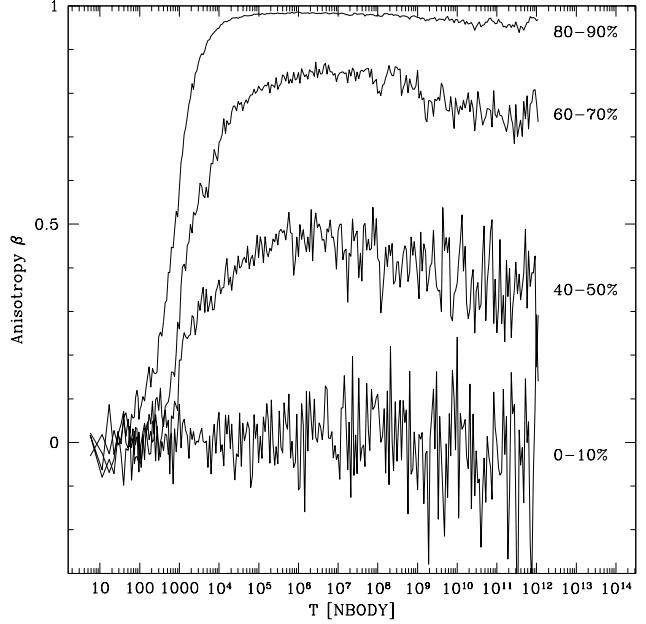


**Figure 17.** Evolution of the anisotropy with time for 4 different radii for clusters with  $N = 4096$  stars. Clusters are strongly anisotropic in their outer parts but remain isotropic near their centers. The mean anisotropy increases up to  $10^6$   $N$ -body time units and decreases slowly afterwards. A similar behavior is found for other particle numbers.

weakly bound stars as the particle numbers drop. Stars with energies near  $E = 0$  are predominantly on near radial orbits when closer to the cluster center. The removal of such stars must therefore decrease the anisotropy at intermediate radii.

We can compare the anisotropy profile for clusters with different particle numbers by binning data from several snapshots around the time when the clusters reach maximum anisotropy. Fig. 18 shows the resulting profiles as a function of enclosed mass. The anisotropy rises monotonically from the core, which is isotropic for all  $N$ , towards the halo. For large  $N$ , the differences become smaller and it might be possible that the profiles are converging towards a maximum profile at the high- $N$  end. Unfortunately it is difficult to say if this is really the case, due to the small number of simulations made (only one for  $N = 8192$ ) and the resulting uncertainties in the profiles. If so, it would mean that there is an universal density and velocity profile, which only clusters with large enough  $N$  can reach, since the evolution of low- $N$  models towards this profile is interrupted by the removal of their outer halo.

It was already shown that the cluster expansion is driven by encounters of stars near the 10% lagrangian radius (Fig. 2). Hence, the 10% lagrangian radius should also play an important role for the anisotropy profile. Fig. 19 depicts the anisotropy profile for different particle numbers, calculated by dividing the radii of each model by its 10% lagrangian radius. It can be seen that the profiles are nearly the same for all  $N$ , showing again that the 10% radius is the radius where halo stars are created. We found that no other radius leads to such an agreement in the profiles.

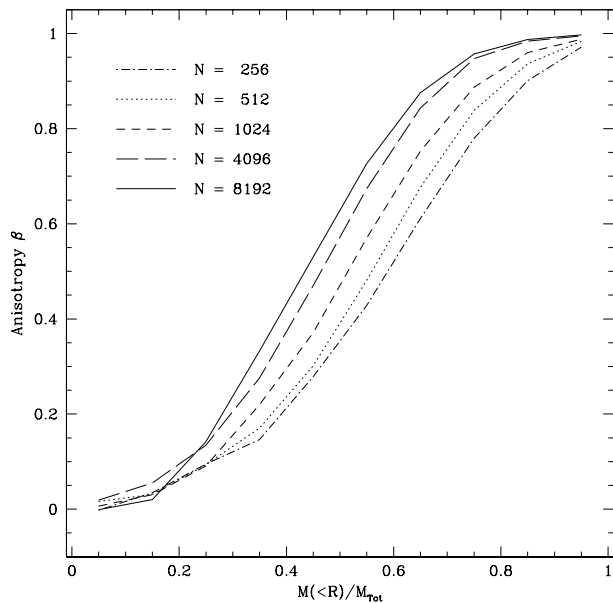


**Figure 18.** Maximum anisotropy in dependence of the initial number of cluster stars. The anisotropy is plotted as a function of enclosed mass. Shown are curves from  $N = 256$  (bottom) to  $N = 8192$  (top). The anisotropy in the halo increases with increasing particle number.

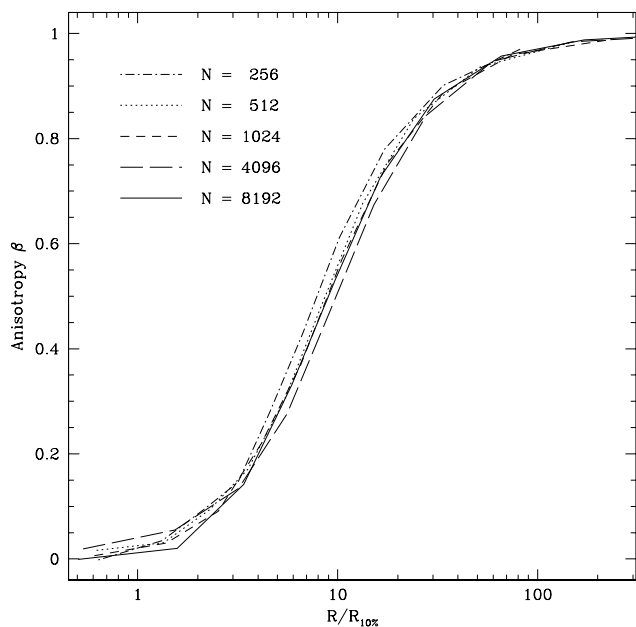


**Figure 19.** Maximum anisotropy as a function of distance to the cluster center. If distances are scaled by the 10% lagrangian radius, the anisotropy profile is independent of the particle number. Most stars should therefore be scattered into the halo from around this radius.

Hénon (1973) found that spherical stellar systems with radially anisotropic distribution functions can be vulnerable to radial orbit instabilities. His results were later confirmed and extended by Barnes, Hut & Goodman (1986) and Dejonghe & Merritt (1988). Dejonghe & Merritt (1988) found that models based on Plummer’s density law become unstable if the global anisotropy exceeds a critical value of  $2T_r/T_t \approx 2.0$ . The anisotropies in our highest- $N$  models are close to this value, and so it might be interesting to look for signs of such instabilities in our runs.

We calculated for all models with  $N \geq 1024$  and all times when data was stored the moment of inertia tensor of the stellar distribution and its eigenvectors and eigenvalues. We studied only radial shells between the 20% and 80% lagrangian radius, since the velocity distribution is isotropic for smaller radii. Since previous work indicates that radially anisotropic stellar systems develop bar-like mass distributions, we first checked for stellar bars in our models.

Fig. 20 shows for the 8K run the angular distribution of the eigenvectors which belong to the smallest moment of inertia. It can be seen that their distribution is more or less random. This is not what one would expect in the presence of radial orbit instabilities, since bar-like configurations should have fixed axes in space, at least for a certain amount of time. In a second test we compared the ratio of the smallest eigenvalue to the sum of the other two. If a cluster collapses into a bar-like configuration, one would expect to see a sudden drop of this ratio. However, no such drop could be seen anywhere in the run. Hence no signs of instabilities could be found in the 8K run and similar results were obtained for runs with smaller particle numbers. We also found no signs for disc-like instabilities in any of our runs.

There are several possible explanations for the absence of radial orbit instabilities: Our distributions might not be anisotropic enough to become unstable, or relaxation processes suppress them since they tend to make distributions spherical. Most important for halo stars are passages through the inner cluster parts, where encounters with other stars can significantly change their orbits. As was shown earlier (Fig. 3), the relaxation times in the center change only slowly with the particle number since high- $N$  clusters are more concentrated. The onset of radial orbit instabilities might therefore be suppressed by relaxation processes in the cluster center, no matter how large  $N$  becomes.

A third possibility is that the halo is constantly renewed and extended by stars ejected from the cluster center. Since such stars will be scattered uniformly in all directions, they can also prevent the formation of structures in the halo.

## 4 CONCLUSIONS

We have performed a set of  $N$ -body simulations of isolated single-mass clusters starting from Plummer profiles. Our main focus was on the post-collapse evolution, and for the first time we could follow this evolution until nearly complete disintegration of the clusters, thereby extending the parameter space of collisional stellar dynamics significantly.

We found that after a sufficient number of relaxation times has passed, the structure of the clusters becomes independent of the initial density profile and particle number, and can be characterized by just two parameters, as e.g. the

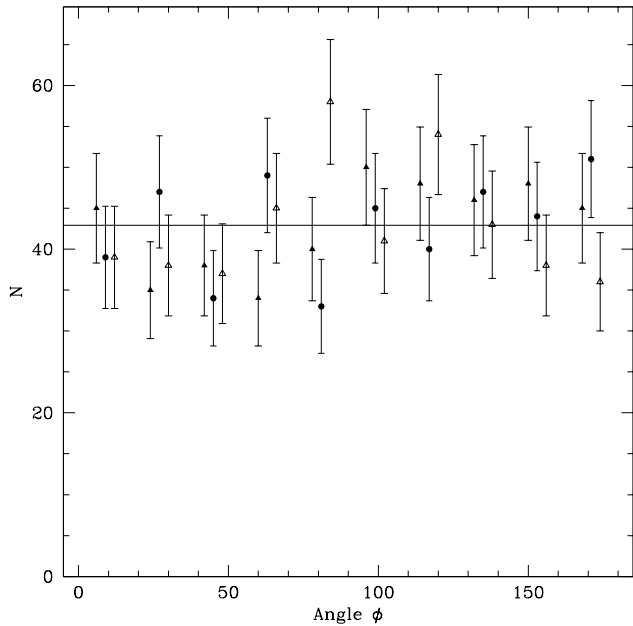


**Figure 20.** Angular distribution of the eigenvectors that belong to the smallest eigenvalue for the 8K run. Circles show the projection into the x-y plane, open triangles into the x-z plane and filled triangles into the y-z plane. The solid line shows the expected value for a uniform distribution. The distribution of the data from the  $N$ -body run is compatible with a random distribution.

actual particle number and the half-mass radius. For very large  $N$ , the cluster structure might become independent of the actual particle number too, although our simulations could not reach large enough  $N$  to test this assumption. We found that isolated clusters evolve along a single sequence of models and runs starting from different particle numbers can be stitched together. This can be relevant for the post-collapse evolution of galactic globular clusters which have half-mass radii much smaller than their tidal radii, since these systems would be nearly isolated and might have profiles similar to our models.

We found that low- $N$  clusters have larger radii after core collapse, so that all clusters have similar relaxation times during the post-collapse expansion phase. As a consequence, the mass-loss rates depend only weakly on the particle number. Due to their higher concentration, high- $N$  clusters loose mass even faster than low- $N$  models.

Stars in isolated clusters are ejected almost entirely from within the half-mass radius, with encounters between single stars being the dominant escape mechanism. We could establish a clear correlation between the excess energy of escapers and the position where the escapers are created. Such a relation could also exist for clusters in tidal fields, although the long time necessary for escape complicates the escape of stars in this case (Fukushige & Heggie 2000, Baumgardt 2001).

For all clusters, only a few binaries are present and drive the expansion. Their fraction decreases with increasing particle number, while the total number increases roughly as  $N_{Bin} \sim N^{0.3}$ . About 15% of the stars are ejected due to

encounters with binaries and these carry away a large fraction of the cluster energy. Binaries are strongly concentrated towards the cluster cores, and the ejection by binaries also happens only near the cluster centers. For clusters showing core oscillations, binary induced escape is efficient only in the contraction phases of the core, while the escape due to single-star encounters fluctuates much less with the core oscillations.

A radially anisotropic velocity distribution is created in the cluster halos, mainly as a result of two-body encounters near the 10% lagrangian radius. High- $N$  clusters have smaller core sizes and show therefore larger overall anisotropies. It seems conceivable that isolated clusters are vulnerable to radial orbit instabilities for sufficiently large  $N$ , but no indication for such instabilities could be found.

## ACKNOWLEDGMENTS

We are grateful to Rainer Spurzem for his help with the NBODY6++ code and to Jun Makino for useful discussions. We would also like to thank an anonymous referee for comments which improved the presentation of the paper. It is a pleasure to acknowledge the support of the European Commission through TMR grant number ERB FMGE CT950051 (the TRACS Programme at EPCC). The parallel computations were performed on the CRAY T3E of HLRS Stuttgart. H.B. was supported by PPARC under grant 1998/00044.

## REFERENCES

- Aarseth S., 1971, *Ap&SS* 13, 324
- Aarseth S., 1999, *PASP* 111, 1333
- Antonov V. A., 1962, *Vestnik Leningrad Univ.*, 7, 135
- Barnes J., Hut P., Goodman J., 1986, *ApJ* 300, 112
- Baumgardt H., 2001, *MNRAS* 325, 1323
- Binney J., Tremaine S., 1987, *Galactic Dynamics*, Princeton Univ. Press, Princeton
- Breeden J. L., Cohn H. N., Hut P., 1994, *ApJ* 421, 195
- Casertano S., Hut P., 1985, *ApJ* 298, 80
- Cohn H., 1985, in Goodman J., Hut P. (eds), *IAU Symposium* 113, *Dynamics of Star Clusters*, Kluwer, Dordrecht, p. 161
- Dejonghe H., Merritt D., 1988, *ApJ* 328, 93
- Drukier G. A., Cohn H. N., Lugger P. M., Yong H., 1999, *ApJ* 518, 233
- Fukushige T., Heggie D.C., 2000, *MNRAS* 318, 753
- Giersz M., Heggie D. C., 1994a, *MNRAS* 268, 257
- Giersz M., Heggie D. C., 1994b, *MNRAS* 270, 298
- Giersz M., Heggie D. C., 1997, *MNRAS* 286, 709
- Giersz M., Spurzem S., 1994, *MNRAS* 269, 241
- Giersz M., Spurzem S., 2000, *MNRAS* 317, 581
- Goodman J., 1984, *ApJ* 280, 298
- Goodman J., 1987, *ApJ* 313, 576
- Heggie D. C., 1975, *MNRAS* 173, 729
- Hénon M., 1960, *Ann. Astrophys.* 23, 668
- Hénon M., 1973, *A&A* 24, 229
- Inagaki S., Lynden-Bell D., 1983, *MNRAS* 205, 913
- Larson R. B., 1970, *MNRAS* 150, 93
- Lightman A. P., Shapiro S. L., 1978, *Rev. Mod. Phys.* 50, 437
- Lynden-Bell D., Eggleton P. P., 1980, *MNRAS* 191, 483
- Lynden-Bell D., Wood R., 1968, *MNRAS* 138, 495
- Makino, J., 2001, in *Dynamics of Star Clusters and the Milky Way*, eds. S. Deiters, B. Fuchs, A. Just, R. Spurzem, R. Wielen, ASP Conference Series 228, p. 87

- Makino J., 2002, in *Astrophysical Supercomputing using Particle Simulations*, eds. J. Makino, P. Hut, IAU Symposium 208, in preparation
- Makino J., Aarseth S.J., 1992, PASJ 44, 141
- Spitzer L. Jr., Shapiro S. L., 1972, ApJ 173, 529
- Spitzer L. Jr., 1987, *Dynamical Evolution of Globular Clusters*, Princeton University Press, Princeton
- Spurzem R., 1999, in Riffert H., Werner K. (eds), *Computational Astrophysics, The Journal of Computational and Applied Mathematics (JCAM)* 109, Elsevier Press, Amsterdam, p. 407
- Spurzem R., Aarseth S. J., 1996, MNRAS 282, 19
- Spurzem R., Baumgardt H., 2002, MNRAS submitted
- Takahashi K., 1995, PASJ 47, 561
- Takahashi K., 1996, PASJ 48, 691
- Takahashi K., Portegies Zwart S. F., 2000, ApJ 535, 759

This paper has been produced using the Royal Astronomical Society/Blackwell Science L<sup>A</sup>T<sub>E</sub>X style file.